Journal of Physics and Chemistry of Solids 75 (2014) 136–141

Contents lists available at ScienceDirect

Journal of Physics and Chemistry of Solids

journal homepage: www.elsevier.com/locate/jpcs

Single-crystal elastic constants of magnesium difluoride (MgF_2) to 7.4 GPa

Ilias S. Zouboulis [1], Fuming Jiang, Jue Wang, Thomas S. Duffy *

Department of Geosciences, Princeton University, Princeton, NJ 08544, USA

ARTICLE INFO

Article history:
Received 1 June 2013
Received in revised form
13 August 2013
Accepted 14 September 2013
Available online 20 September 2013

Keywords:
C. High pressure
D. Phase transition
D. Electrical properties
D. Equations-of-state

ABSTRACT

The six independent elastic constants (C_{11}, C_{12}, C_{13}, C_{33}, C_{44}, and C_{66}) of single-crystal MgF_2 in the rutile structure have been measured by Brillouin spectroscopy at room temperature from ambient conditions to 7.4 GPa. Measurements were performed on two monocrystals with perpendicular faces, (001) and (100). A quasi-linear fit from finite strain theory was applied to the experimental data revealing the pressure dependence of the six elastic constants of MgF_2. The shear modulus $C_S=1/2(C_{11}-C_{12})$, and the aggregate shear (Voigt–Reuss–Hill) modulus G show a softening with increasing pressure, indicating the approach of the rutile-to-$CaCl_2$-type structural phase transition at $P\sim9$ GPa. The adiabatic bulk modulus (Reuss average) and its pressure derivative have been determined: $K_{0S}=105.1\pm0.3$ GPa, $(\partial K_{0S}/\partial P)_T=4.14\pm0.05$. The pressure–volume equation of state of MgF_2 was computed self-consistently from the Brillouin data. Our results are in good agreement with X-ray diffraction data. As the phase transition is approached, MgF_2 becomes strongly anisotropic and develops partially auxetic behavior (a negative Poisson's ratio in certain directions).

1. Introduction

Magnesium difluoride (MgF_2, sellaite) is a simple, archetypical ionic crystal. It has been used extensively in technical applications as an optical material, due to its transparency to a very broad continuous wavelength range, from the vacuum ultraviolet ($\sim$0.120 μm) to the mid-infrared ($\sim$8.0 μm) [22]. There has been strong interest in understanding its high-pressure phase transition. Under ambient conditions it crystallizes in the tetragonal system, having the rutile structure (point group: 4/mmm, space group: $P4_2/mnm$ or D_{4h}^{14}, with two formula units per unit cell, $Z=2$). This means that it is isostructural to many other AB_2 compounds, among them oxides (rutile TiO_2, stishovite SiO_2, argutite GeO_2 and cassiterite SnO_2) and difluorides (MnF_2, FeF_2, CoF_2, NiF_2 and ZnF_2). Due to the valence and the ionic radius of the F^- ion, MgF_2 should be elastically weaker than its isostructural oxides, showing similar elastic behavior and mode softening, but at much lower pressures. On the other hand, since the Mg^{2+} ion has no d electrons, it is expected to have a more ionic character and a more stable structure than its isostructural transition-metal difluorides.

Extensive theoretical and experimental studies have revealed that these compounds may undergo a series of phase transitions under the influence of pressure. The most common is the pressure-induced phase transition to a structure closely related to the initial rutile, the orthorhombic $Pnnm$ ($Z=2$) $CaCl_2$ structure, which takes place around 9 GPa in MgF_2 [8]. According to Landau theory, this phase transition should be ferroelastic and of second order [21]. This transition is characterized by the pressure dependence of the elastic shear modulus, $C_S=1/2(C_{11}-C_{12})$, which describes the softening behavior of the transverse acoustic soft mode along {110} with B_{1g} symmetry.

Previously, the pressure dependence of the elastic moduli of single-crystal MgF_2 was measured ultrasonically only up to a maximum pressure of 10 kbar or 1 GPa [25]. It is interesting to note that the elastic shear modulus C_S begins to show nonlinearity and negative slope characteristics with increasing pressure even at this low pressure range. These traits are early signs of the rutile-to-$CaCl_2$ structure phase transition which eventually takes place at $P\sim9$ GPa [8].

In this paper we report detailed acoustic velocity measurements of two single crystals of MgF_2, with perpendicular (001) and (100) faces. This procedure leads us to the determination of the pressure dependence of the six independent elastic constants of MgF_2, namely C_{11}, C_{12}, C_{13}, C_{33}, C_{44}, and C_{66}, from ambient pressure up to $P=7.4$ GPa. A quasi-linear fit from finite strain theory was applied to the experimental data revealing the pressure dependence of the six elastic constants of MgF_2. The pressure dependence of the elastic

* Corresponding author. Tel.: +1 609 258 6769.
E-mail address: duffy@princeton.edu (T.S. Duffy).
[1] On leave from National Technical University, School of Applied Sciences, Department of Physics, Zografou 15780, Greece.

0022-3697/$ - see front matter © 2013 Elsevier Ltd. All rights reserved.
http://dx.doi.org/10.1016/j.jpcs.2013.09.014

shear modulus C_S, as well as the pressure dependence of the aggregate (Voigt–Reuss–Hill) shear modulus G depart appreciably from linearity in this pressure range (0–7.4 GPa).

2. Experimental procedure

Two double-side polished synthetic single MgF_2 crystals, with (001) and (100) orientations, were purchased from MTI Corp. First, ambient acoustic velocities were measured as a function of azimuthal angle in both crystals. The two crystals were then polished to a thickness ≤ 40 μm, and crystal platelets, with sizes $\sim 100 \times 100$ μm^2, were loaded in a modified, short-piston cylinder, four-screw Mao and Hemley diamond anvil cell [15] with an 96° aperture angle. A cylindrical sample chamber was obtained by machining a 250-μm diameter hole in a stainless steel gasket preindented to a thickness of 50 μm. The sample was compressed between 500-μm diameter culets, and a 16:3:1 volume mixture of methanol, ethanol and water was used as a pressure-transmitting medium. This mixture is known to remain fluid and provide hydrostatic conditions to at least 10 GPa [1]. Ruby chips were used as pressure markers. Pressure was calculated from the ruby fluorescence $R1$ line shift [2,14].

Brillouin scattering experiments were performed in a forward symmetric (platelet) geometry, which allows determination of the acoustic velocity independent of the refractive index of the sample [26]. The inelastic Brillouin scattering effect was excited using 160 mW of a frequency-doubled, vertically polarized neodymium vanadate laser ($\lambda_0 = 532.15$ nm), measured using a six-pass tandem Fabry–Perot interferometer [13], and recorded by a solid-state photon detector with 70% quantum efficiency in the frequency range of interest. The signal was processed through a multichannel analyzer and stored in digital form. A diagram of the experimental set-up is shown elsewhere [23]. Measurements were performed up to 7.4 GPa. At higher pressures, we observed anomalous velocities, presumably because of complex structural changes associated with the phase transition, and here we report only data that are unambiguously in the low-pressure phase.

In the forward symmetric or platelet geometry the Brillouin frequency shift $\Delta\nu$ is related to the acoustic velocity, v, through the relation

$$v = \Delta\nu\lambda_0/(2 \sin \alpha), \quad (1)$$

where λ_0 is the incident laser wavelength and α is the external incidence angle. In all our measurements an external incidence angle $\alpha = 35°$ was used.

The Brillouin shift corresponding to each channel number i of the spectrum is found as follows:

$$\Delta\nu = [(-A/\lambda_0) + (i-1) \times (2A/\lambda_0)] \times (c/N) \times \text{FSR (in GHz)}, \quad (2)$$

where A is the scanning amplitude of the moving mirrors of the Fabry–Perot interferometer (typical value for this experiment: $A = 560$–600 nm). FSR is the free spectral range of the interferometer:

$$\text{FSR} = 1/(2nD), \quad (3)$$

where n is the index of refraction for the optical medium, which is air in our case, so $n \approx 1$. D is the (total) spacing between the mirrors. In these experiments, $D = 0.5$ cm. c is the velocity of light in vacuum, $c = 3 \times 10^8$ m/s, and N is the total number of channels of the multichannel analyzer.

3. Results and discussion

The longitudinal (C_{11}, C_{33}) shear (C_{44}, C_{66}) and off-diagonal (C_{12}, C_{13}) elastic moduli of single-crystal tetragonal MgF_2, can be determined by measuring the velocities of acoustic waves along at least 2 crystal planes, for example along (001) and (100) planes, to achieve well-constrained elastic constants. Even in this case, the off-diagonal elements C_{12} and C_{13} are more poorly constrained than the longitudinal or shear elements.

Brillouin spectra were collected, from both (001) and (100) face samples, in 20 to 30 crystallographic directions at the following pressures: ambient, 2.0 GPa, 3.9 GPa, 6.2 GPa, and 7.4 GPa. Both quasilongitudinal and quasitransverse modes were detected. A representative spectrum from the (100) sample at the highest pressure, $P = 7.4$ GPa, for which we were able to get reliable data is shown in Fig. 1. The Brillouin peaks corresponding to the pressure-transmitting liquid, MEW, and the Brillouin peaks due to diamond (D) are also shown. The dependence of the acoustic velocities on the direction (expressed by the in-plane azimuthal angle) at the highest pressure, $P = 7.4$ GPa, for the (001) and for the (100) sample are shown in Fig. 2a and b respectively, together with the non-linear least squares fitting-curve, as described below.

The elastic tensor of magnesium difluoride (point group 4/mmm) is characterized by six independent elastic constants, C_{11}, C_{12}, C_{13}, C_{33}, C_{44}, and C_{66} [tetragonal symmetry, class 2) [19]. The acoustic velocity data from the two MgF_2 samples, scattering from their respective (001) and (100) faces, and an initial density, $\rho = 3.178$ g/cm^3 were inverted using a nonlinear least-squares fitting to the Christoffel equation, based on the Levenberg–Marquardt algorithm and the Cardano formulae [6]. The elastic constants were determined to a precision of $\sim \pm 0.5$–1% for at ambient pressures. The precision of the Eulerian orientation angles for the two samples is estimated to be $\pm 3°$. The inverted elastic constants permitted us to calculate the Reuss and Voigt bounds and the Voigt–Reuss–Hill averages [10] of the aggregate bulk and shear moduli at each experimental pressure.

For the determination of the parameters of a Eulerian finite strain (Birch–Murnaghan) equation of state [4] of the individual and aggregate elastic moduli, and for the determination of the density at each pressure, an iterative procedure was followed. The aggregate bulk modulus of MgF_2 and its derivative, K_{0T} and $(\partial K_{0T}/\partial P)_T$, as derived from X-ray diffraction data [8] was first used to calculate the density at each experimental pressure, using the Birch–Murnaghan equation of state [4,18]. Then the Brillouin data were inverted to calculate the high-pressure moduli of MgF_2, from which the Voigt and Reuss bounds and the Voigt–Reuss–Hill average of the adiabatic bulk modulus K_S was calculated at each pressure. These data were fitted to a third-order Birch–Murnaghan equation of state (finite strain equation), from which the zero-pressure adiabatic bulk modulus and its derivative, K_{0S} and $(\partial K_{0S}/\partial P)_T$, were obtained. The correction from adiabatic to isothermal values of these quantities

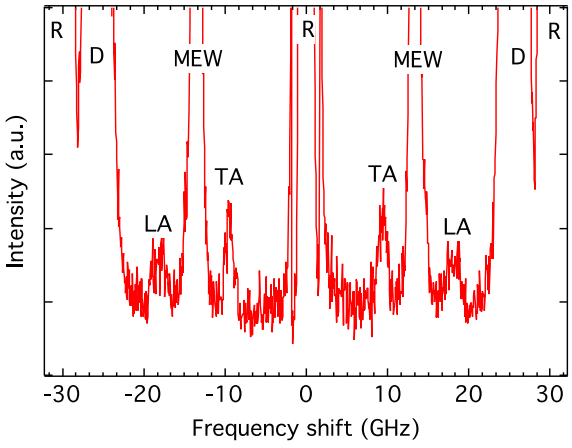

Fig. 1. Representative spectrum of MgF_2 in the (100) plane, collected at $P = 7.4$ GPa. *LA*: quasi-longitudinal acoustic mode; *TA*: quasi-transverse acoustic mode; *MEW*: peaks from the ethanol–methanol–water pressure transmitting medium; *D*: peaks from diamond; and *R*: unshifted Rayleigh line.

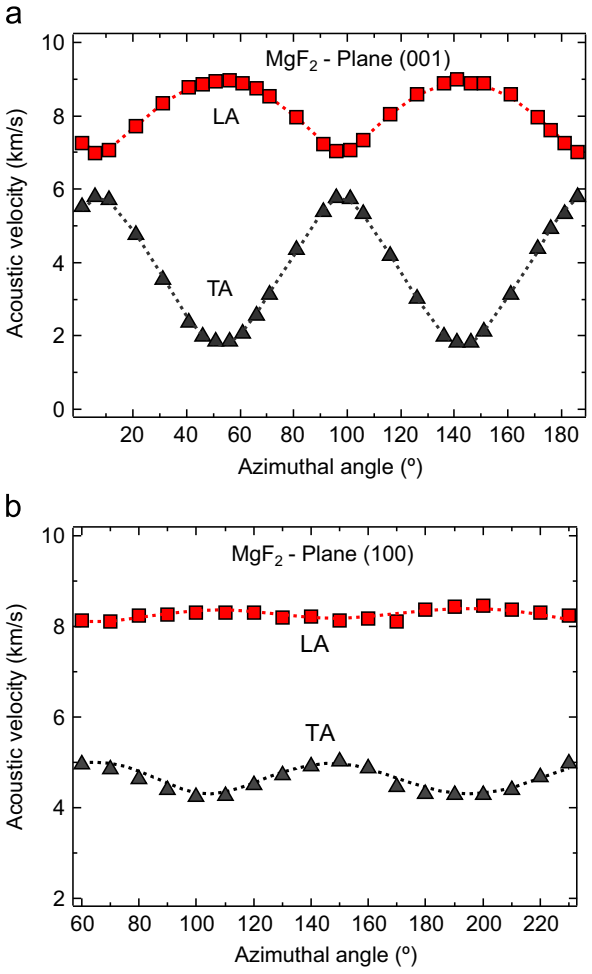

Fig. 2. Quasilongitudinal and quasitransverse acoustic velocities at 7.4 GPa as a function of crystallographic direction in the (a) (001) and (b) (100) plane. The azimuthal angle is relative to an arbitrary starting direction an the corresponding plane. The dashed curves are calculated using the best-fit elastic constants, derived from the acoustic velocity data through inversion of the Christoffel equation. Abbreviations are as in Fig. 1.

Table 1
Thermodynamic and thermoelastic parameters of MgF_2 under ambient conditions. ρ_0: Density at ambient conditions (Mg/m^3), T: temperature (K). .
Source: Sumino and Anderson [24]

Parameter	Value
Thermal expansivity (α)	$37.7\times10^{-6}\,K^{-1}$
Grüneisen parameter (γ)	1.2
$(\partial K_{0T}/\partial T)_P$	-0.02 GPa/K
Conversion formulas :	
$K_{0T}=K_{0S}/(1+\alpha\gamma T)$	
$(\partial K_{0T}/\partial P)_T \approx \{(\partial K_{0S}/\partial P)_T-[(\gamma T/K_{0T})\times(\partial K_{0T}/\partial T)_P]\}/(1+\alpha\gamma T)$	

was done using known values of various thermodynamic parameters of MgF_2. (See Table 1 for these values, and for the conversion formulas from the isentropic to the isothermal parameters). This procedure led us again to the ambient-pressure isothermal values, K_{0T} and $(\partial K_{0T}/\partial P)_T$, (Reuss bounds) from which the density was recalculated from the Birch–Murnaghan equation of state. This iterative procedure was continued, until the density converged. Next, the $C_{ij}-\rho$ data were fit to the finite strain equations [4] yielding the fit values of the individual moduli at ambient conditions and their pressure derivatives.

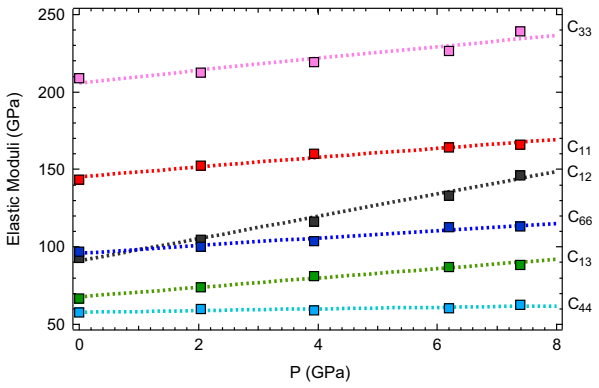

Fig. 3. Elastic moduli of MgF_2 as functions of pressure. Squares are measurements from this study. The dashed lines are third order Eulerian finite strain fits to the individual moduli. Uncertainties are smaller than the dimensions of the squares representing the experimental points.

It is interesting to note that the equation of state, as derived iteratively above, is independent of the initial equation of state, with the exception of the density at ambient (zero) pressure. The inversion procedure in this case converged to the final solution after two iterations, starting from the equation of state derived from values for the K_{0T} and the derivative $(\partial K_{0T}/\partial P)_T$ [8].

The pressure dependence of the six independent elastic constants of MgF_2 is shown in Fig. 3, together with a quasi-linear fit to the experimental data (dashed lines) from finite strain theory. The measured values of the elastic constants at each pressure are also shown in Table 2. The uncertainties of the elastic constants, representing one standard deviation σ from the inverted value, are: $\Delta C_{11}=\pm1.0\%$, $\Delta C_{33}=\pm1.2\%$, $\Delta C_{12}=\pm1.3\%$, $\Delta C_{13}=\pm3.6\%$, $\Delta C_{44}=\pm1.8\%$ and $\Delta C_{66}=\pm1.4\%$ for the highest pressure, $P=7.4$ GPa, of our experiments. Our results for the pressure derivatives $\partial C_{11}/\partial P$, $\partial C_{12}/\partial P$, $\partial C_{33}/\partial P$, $\partial C_{44}/\partial P$, and $\partial C_{66}/\partial P$, are significantly lower than the corresponding ultrasonic values [25]. Only $\partial C_{44}/\partial P$ appears to be larger, as derived from the ultrasonics measurements, than the corresponding $\partial C_{44}/\partial P$ value acquired from the Brillouin measurements. At this point it is useful to note that ultrasonic measurements extend to pressures up to 1 GPa only.

The values of the Reuss and Voigt bounds and the Voigt–Reuss–Hill isentropic bulk moduli were calculated from the corresponding values of the elastic constants at the experimental pressures $P=0$ GPa, (ambient) $P=2.0$ GPa, $P=3.9$ GPa, $P=6.2$ GPa, and $P=7.4$ GPa, using the formulae [17]:

$$K_V=[2(C_{11}+C_{12})+C_{33}+4C_{13}]/9, \tag{4}$$

$$K_R=[(C_{11}+C_{12})C_{33}-2C_{13}^2]/(C_{11}+C_{12}+2C_{33}-4C_{13}) \tag{5}$$

$$K_H=(K_V+K_R)/2 \tag{6}$$

The Reuss-bound data were fitted to a third-order Birch–Murnaghan equation of state for the isentropic bulk modulus of MgF_2 [4]:

$$K_S=(1+2f)^{5/2}\{K_{0S}+[3K_{0T}(\partial K_{0S}/\partial P)_T-5K_{0S}]f\}, \tag{7}$$

where f is the Eulerian strain:

$$f=(1/2)\times[(V_0/V)^{2/3}-1]=(1/2)\times[(\rho/\rho_0)^{2/3}-1]. \tag{8}$$

From this fit we obtained the (Reuss-bound) values of K_{0S} and $(\partial K_{0S}/\partial P)_T$ for MgF_2:

$K_{0S}=105.1\pm0.3$ GPa, $(\partial K_{0S}/\partial P)_T=4.14\pm0.05$

The isothermal values K_{0T} and $(\partial K_{0T}/\partial P)_T$ were derived using the thermodynamic and thermoelastic parameters of MgF_2 as listed in

Table 2
Elastic moduli of MgF_2 as functions of pressure.

P (GPa)	C_{11} (GPa)	C_{33} (GPa)	C_{12} (GPa)	C_{13} (GPa)	C_{44} (GPa)	C_{66} (GPa)
0	143.5	208.8	93.0	66.9	57.8	96.9
2.0	152.4	212.5	104.7	74.0	59.8	100.1
3.9	160.1	219.1	116.3	81.1	59.0	103.8
6.2	164.4	226.3	133.2	87.2	60.5	112.7
7.4	166.3	239.4	145.8	88.2	62.7	113.7

At elevated pressures, uncertainties are 1–2% for the longitudinal (C_{11}, C_{33}) and shear moduli (C_{44}, C_{66}), and up to 4% for the off-diagonal moduli (C_{12}, C_{13}).

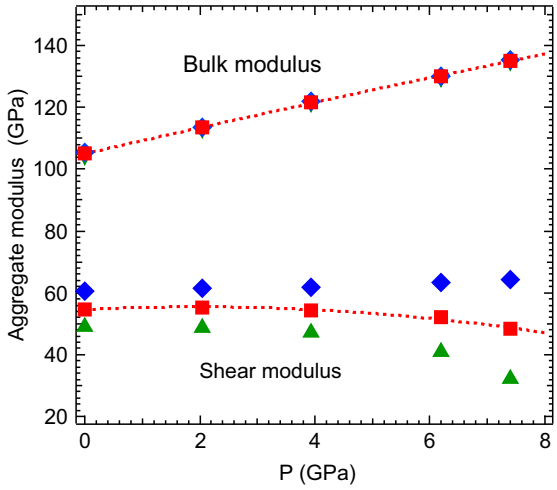

Fig. 4. Adiabatic aggregate bulk and shear moduli of MgF_2 as a function of pressure. The red squares represent the Hill-average adiabatic bulk and shear moduli from our data, green triangles and blue diamonds represent the Reuss bound and the Voigt bound adiabatic bulk and shear moduli from our data, respectively. The red dashed lines are fits to the Hill-average experimental data in the two cases. Uncertainties are smaller than the dimensions of the symbols representing the experimental points. (For interpretation of the references to color in this figure legend, the reader is referred to the web version of this article.)

Table 1, and then following the iterative procedure already described. The isothermal bulk modulus is 1.4% less than the adiabatic bulk modulus. The final values are:

$K_{0T} = 103.7 \pm 0.3$ GPa, $(\partial K_{0T}/\partial P)_T = 4.15 \pm 0.05$.

The pressure dependence of the isentropic bulk modulus, $K_S(P)$, of MgF_2, as derived from our C_{ij} measured values, is shown in Fig. 4. We note that the difference between the Voigt K_V and Reuss K_R bulk moduli, differ only by $<1\%$ at all pressures ($\sim$1 GPa or less). The values of K_{0T} and $(\partial K_{0T}/\partial P)_T$, for MgF_2, as derived in this study, are compared with the corresponding values obtained in previous theoretical and experimental studies in Table 3. It is easy to deduce from this table that our experimental values are better constrained than the bulk modulus and its derivative derived from ultrasonics or X-ray diffraction data. This is due to the inherent features of the fitting procedure used to derive these results. In this case the uncertainty is deduced statistically, from the 1σ standard deviation of the numerical results obtained through the fitting algorithm. This feature is also clearly seen in Fig. 5, in which the equation-of-state curve is shown [3,8]:

$$P = (3/2)K_{0T}[(V_0/V)^{7/3} - (V_0/V)^{5/3}] \times [1 + (3/4[(\partial K_{0T}/\partial P)_T - 4] \times [V_0/V)^{2/3} - 1] \quad (9)$$

The (Reuss bound) isothermal bulk modulus K_{0T} and its derivative, $(\partial K_{0T}/\partial P)_T$, as derived from our data [red symbols] and from Haines's X-ray diffraction data [black symbols] were used to plot the corresponding fitting curves [red dashed line: fit to our data, black dashed line: fit to Haines's data]. It is clear that in this

Table 3
Measured bulk modulus (Reuss bound) K_{0T} and its pressure derivative, $(\partial K_{0T}/\partial P)_T$ of MgF_2.

	K_{0T} (GPa)	$(\partial K_{0T}/\partial P)_T$
Present work (Brillouin)	103.7 ± 0.3	4.15 ± 0.05
[25] (Ultrasonics)	100.3	3.8
[8] (X-ray diffraction)	101 ± 3	4.2 ± 1.1
[27] (Theory)	97	3.7
[11] (Theory)	101	
[5] (Theory)	105	

Measured adiabatic moduli have been converted to isothermal moduli. Theoretical values are at 0 K.

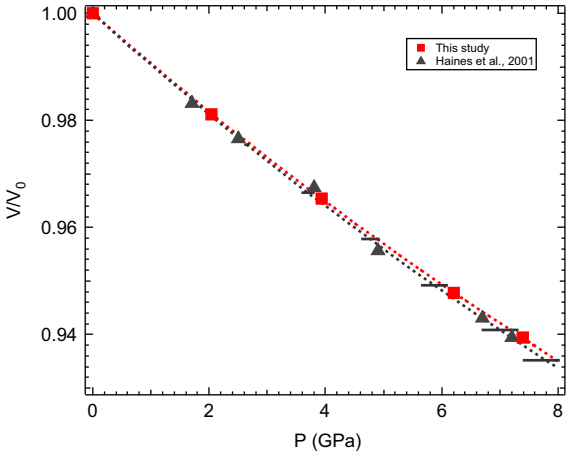

Fig. 5. Birch–Murnaghan equation of state for MgF_2 (unit cell volume normalized to ambient unit cell volume). The red squares represent our Brillouin spectroscopy measurements, and the red dashed line is a third-order finite strain fit to these data. The black triangles are X-ray diffraction experimental data [8], and the black dashed line is a fit to these diffraction data. The experimental error bars are smaller than the dimensions of the symobls. The black error bar refers to the dashed black line, being derived by error propagation. It is calculated from the uncertainties of the bulk modulus and of the pressure derivative of the bulk modulus from the X-ray data [8]. (For interpretation of the references to color in this figure legend, the reader is referred to the web version of this article.)

pressure range the difference in the value of P for a given V/V_0 between the two curves is $\sim$0.1 GPa ($\sim$1.5%), which is comparable to the experimental error for the pressure determination. However, our curve is much better constrained than Haines's equation of state.

The values of the Voigt–Reuss–Hill isentropic shear modulus were calculated from the corresponding values of the elastic constants at each pressure using the formulae [17]:

$$G_V = (4C_{11} - 2C_{12} - 4C_{13} + 2C_{33} + 12C_{44} + 6C_{66})/30 \quad (10)$$

$$G_R = 15/\{18K_V/[(C_{11} + C_{12})C_{33} - 2C_{13}^2] + 6/(C_{11} - C_{12}) + 6/C_{44} + 3/C_{66}\}. \quad (11)$$

$$G_H = (G_V + G_R)/2 \quad (12)$$

The resulting values of the isentropic shear moduli are shown in Fig. 4.

The values of the shear modulus $C_S = (C_{11} - C_{12})/2$ were calculated from the corresponding values of the elastic constants C_{11} and C_{12} (Fig. 6). Both the aggregate shear modulus and C_S soften with increasing pressure, showing that there is an imminent phase transition. Extrapolation of the trend in C_S results in this quantity reaching zero at $\sim$9.5 GPa. This phase transition is the well-known second order, ferroelastic rutile-to-$CaCl_2$ transition which has been already studied both theoretically [27] and by X-ray diffraction experiments [8] for MgF_2. The softening of the shear modulus C_S is

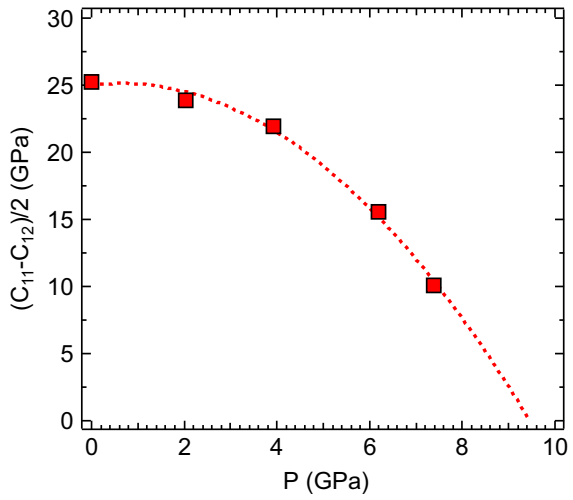

Fig. 6. Shear elastic constant $C_S=(C_{11}-C_{12})/2$ of MgF_2 as a function of pressure. The solid squares are our experimental data. The dashed line is a fit through our data. The error bars are smaller than the dimensions of the squares representing the experimental points.

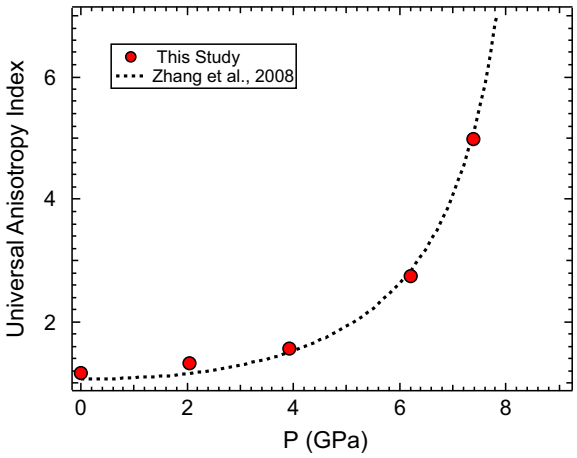

Fig. 7. Elastic anisotropy index $A^U=5G_V/G_R+K_V/K_R-6$ as a function of pressure. The solid circles are our experimental data. The dashed line is derived from an ab initio theoretical calculation of the pressure dependence of the elastic constants of MgF_2 [27]. The error bars are smaller than the dimensions of the circles.

closely related to the behavior of the transverse acoustic Raman active soft mode B_{1g} along {110} [9].

The universal anisotropy index (A^U) is a recently proposed metric for characterizing the elastic anisotropy of crystals of any symmetry [20]. It is simply determined from the Voigt and Reuss bounds on the bulk and shear modulus using the following expression:

$$A^U = 5G_V/G_R+K_V/K_R-6 \geq 0, \quad (13)$$

where the subscript V refers to the Voigt bound and the subscript R refers to the Reuss bound.

In the case of MgF_2, there is a pronounced increase in A^U from a modestly anisotropic value at 1 bar ($A^U=1.2$) to highly anisotropic and increasing rapidly at the highest pressure of this study ($A^U=5.0$). The universal anisotropy index of MgF_2 as a function of pressure, calculated from our experimental data, is shown in Fig. 7. Large values of anisotropy near structural phase transitions have been identified in many materials previously and these are often associated with extreme values of Poisson's ratio as well [12]. Poisson's ratio in an anisotropic elastic material will vary with crystallographic direction. Partially auxetic materials are those for which Poisson's ratio is negative at least in certain directions in the crystal. The directional dependence of Poisson's ratio for MgF_2 was calculated using the program *ElAM* [16]. The minimum Poisson's ratio obtained from our data ranges from 0 at 1 bar to −0.34 at the highest pressure. At 7.4 GPa, the direction of minimum Poisson's ratio is [0.59, 0, −0.81] with the corresponding transverse direction of [−0.81, 0, −0.59]. Thus, MgF_2 becomes strongly auxetic in certain directions under compression as it approaches the rutile-$CaCl_2$ phase transition.

4. Conclusions

We determined the pressure dependence of the six independent elastic moduli of magnesium difluoride in the pressure range from 0 (ambient) to 7.4 GPa. This was achieved by measuring the acoustic velocities of the propagating phonons along two perpendicular [(001) and (100)] planes on two MgF_2 tetragonal monocrystals in a diamond anvil cell by Brillouin spectroscopy. The acoustic velocity data were inverted using a non-linear least-squares fit to the Christoffel equation to provide the six independent elastic moduli at the experimental pressures of the measurements. The finite strain equations were applied to the thus determined individual elastic moduli at each experimental pressure, to obtain the ambient pressure adiabatic individual elastic moduli and their pressure derivatives.

The aggregate bulk modulus of MgF_2 and its pressure derivative was also determined by fitting the experimental data to the finite strain equations. The aggregate isothermal bulk modulus and its pressure derivative was determined: $K_{0T}=(103.7\pm0.3)$ GPa, $(\partial K_{0T}/\partial P)_T=4.15\pm0.05$. These Brillouin scattering data values are inherently better constrained than the corresponding values of the isothermal bulk modulus and its derivative determined by X-ray diffraction data. The error-propagation uncertainties at the experimental points resulting from the third-order Birch–Murnaghan equations of state (EOS) derived from these aggregate values are compared in the two cases. The shear modulus C_S and the aggregate shear (Voigt–Reuss–Hill) modulus G show a softening with increasing pressure, indicating the onset of the imminent rutile-to-$CaCl_2$-structure phase transition at $P\sim9$ GPa. As the phase transition is approached, MgF_2 becomes strongly anisotropic and auxetic, having a negative Poisson's ratio in certain directions.

Acknowledgments

This work was supported by the National Science Foundation and the Carnegie-DOE Alliance Center. I.S.Z. acknowledges financial support from the National Technical University of Athens during his sabbatical stay at Princeton University.

References

[1] R.J. Angel, M. Bujak, J. Zhao, D. Gatta, S.D. Jacobsen, Effective hydrostatic limits of pressure media for high-pressure crystallographic studies, Applied Crystallography 40 (2007) 26–32.
[2] J.D. Barnett, S. Block, G.J. Piermarini, An optical fluorescence system for quantitative pressure measurement in the diamond-anvil cell, Review of Scientific Instruments 44 (1973) 1–9.
[3] F. Birch, Finite elastic strain of cubic crystals, Physical Review 71 (1947) 809–823.
[4] F. Birch, Finite strain isotherm and velocities for single-crystal and polycrystalline NaCl at high pressures and 300 K, Journal of Geophysical Research 83 (1978) 1257–1268.
[5] M. Catti, A. Pavese, R. Dovesi, C. Roetti, M. Causa, Quantum-mechanical Hartree–Fock self-consistent-field study of the elastic constants and chemical bonding of MgF_2 (sellaite), Physical Review B 44 (1991) 3509–3517.
[6] A.G. Every, General closed-form expressions for acoustic waves in elastically anisotropic solids, Physical Review B 22 (1980) 1746–1750.

[8] J. Haines, J.M. Léger, F. Gorelli, D.D. Klug, J.S. Tse, Z.Q. Li, X-ray diffraction and theoretical studies of the high-pressure structures and phase transitions in magnesium fluoride, Physical Review B 64 (2001) (Article no 134110).
[9] H. Hellwig, A.F. Goncharev, E. Gregoryanz, H. Mao, R.J. Hemley, Brillouin and Raman spectroscopy of the ferroelastic rutile-to-$CaCl_2$ transition in SnO_2 at high pressure, Physical Review B 67 (2003) (Article no 174110).
[10] R. Hill, Elastic properties of reinforced solids: some theoretical principles, Journal of the Mechanics and Physics of Solids 11 (1963) 357–372.
[11] V. Kanchana, G. Vaitheeswaran, M. Rajagopalan, High-pressure structural phase transitions in magnesium fluoride studied by electronic structure calculations, Journal of Alloys and Compounds 352 (2003) 60–65.
[12] Z.A.D. Lethridge, R.I. Walton, A.S.H. Marmier, C.W. Smith, K.E. Evans, Elastic anisotropy and extreme Poisson's ratios in single crystals, Acta Materialia 58 (2010) 6444–6451.
[13] S.M. Lindsay, M.W. Anderson, J.R. Sandercock, Construction and alignment of a high-performance multipass Vernier tandem Fabry–Perot interferometer, Review of Scientific Instruments 52 (1981) 1478–1486.
[14] H.K. Mao, J. Xu, P.M. Bell, Calibration of the ruby pressure gauge to 800 kbar under quasi-hydrostatic conditions, Journal of Geophysical Research 91 (1986) 4673–4677.
[15] H.-k. Mao, R.J. Hemley, Experimental studies of Earth's deep interior: accuracy and versatility of diamond anvil cells, Philosophical Transactions of the Royal Society London A 354 (1996) 1315–1332.
[16] A. Marmier, Z.A.D. Lethbridge, R.I. Walton, C.W. Smith, S.C. Parker, K.E. Evans, ElAM: a computer program for the analysis and representation of anisotropic elastic properties, Computer Physics Communications 181 (2010) 2102–2115.
[17] R. Meister, L. Peselnick, Variational method of determining effective moduli of polycrystals with tetragonal symmetry, Journal of Applied Physics 37 (1966) 4121–4125.
[18] F.D. Murnaghan, The compressibility of media under extreme pressures, Proceedings of the National Academy of Sciences 30 (1944) 244–247.
[19] J.F. Nye, Physical Properties of Crystals. Their Representation by Tensors and Matrices, Clarendon Press, Oxford (1985) 140–141.
[20] S.I. Ranganathan, M. Ostoja-Starzewski, Universal elastic anisotropy index, Physical Review Letters 101 (2008) 55504.
[21] E.K.H. Salje, Phase Transitions in Ferroelastic and Coelastic Crystals, Cambridge University Press, Cambridge, 1990.
[22] W.D. Scott, Purification, growth of single crystals, and selected properties of MgF_2, Journal of the American Ceramic Society 12 (1962) 586–587.
[23] S. Speziale, T.S. Duffy, Single-crystal elastic constants of fluorite (CaF_2) to 9.3 GPa, Physics and Chemistry of Minerals 29 (2002) 465–472.
[24] Y. Sumino, O.L. Anderson, Elastic constants of minerals, in: R.S. Carmichael (Ed.), CRC Handbook of Physical Properties of Rocks, CRC, Boca Raton, FL, 1984, pp. 39–138.
[25] J.K. Vassiliou, Pressure dependence of the elastic moduli of single crystal MgF_2 to 1 GPa, Journal of Applied Physics 57 (1985) 4543–4547.
[26] C.H. Withfield, E.M. Brody, W.A. Bassett, Elastic moduli of NaCl by Brillouin scattering at high pressure in a diamond-anvil cell, Review of Scientific Instruments 47 (1976) 942–947.
[27] L. Zhang, Y. Wang, T. Cui, Y. Ma, G. Zou, First principles study of the pressure-induced rutile-$CaCl_2$ phase transition in MgF_2, Solid State Communications 145 (2008) 283–287.